Sensory computations in the cuneate nucleus of macaques

Aneesha K. Suresh[a,1], Charles M. Greenspon[b,1], Qinpu He[a], Joshua M. Rosenow[c], Lee E. Miller[d,e,f,g], and Sliman J. Bensmaia[a,b,h,2]

[a]Committee on Computational Neuroscience, University of Chicago, Chicago, IL 60637; [b]Department of Organismal Biology and Anatomy, University of Chicago, Chicago, IL 60637; [c]Department of Neurological Surgery, Feinberg School of Medicine, Northwestern University, Chicago, IL 60611; [d]Department of Physiology, Feinberg School of Medicine, Northwestern University, Chicago, IL 60611; [e]Department of Physical Medicine and Rehabilitation, Feinberg School of Medicine, Northwestern University, Chicago, IL 60611; [f]Department of Biomedical Engineering, McCormick School of Engineering, Northwestern University, Evanston, IL 60208; [g]Shirley Ryan AbilityLab, Chicago, IL 60611; and [h]Grossman Institute for Neuroscience, Quantitative Biology, and Human Behavior, University of Chicago, Chicago, IL 60637

Edited by Jon H. Kaas, Vanderbilt University, Nashville, TN, and approved October 27, 2021 (received for review August 29, 2021)

Tactile nerve fibers fall into a few classes that can be readily distinguished based on their spatiotemporal response properties. Because nerve fibers reflect local skin deformations, they individually carry ambiguous signals about object features. In contrast, cortical neurons exhibit heterogeneous response properties that reflect computations applied to convergent input from multiple classes of afferents, which confer to them a selectivity for behaviorally relevant features of objects. The conventional view is that these complex response properties arise within the cortex itself, implying that sensory signals are not processed to any significant extent in the two intervening structures—the cuneate nucleus (CN) and the thalamus. To test this hypothesis, we recorded the responses evoked in the CN to a battery of stimuli that have been extensively used to characterize tactile coding in both the periphery and cortex, including skin indentations, vibrations, random dot patterns, and scanned edges. We found that CN responses are more similar to their cortical counterparts than they are to their inputs: CN neurons receive input from multiple classes of nerve fibers, they have spatially complex receptive fields, and they exhibit selectivity for object features. Contrary to consensus, then, the CN plays a key role in processing tactile information.

touch | neural coding | receptive fields | vibration | integration

The coding of tactile information has been extensively studied in the peripheral nerves and in the primary somatosensory cortex (S1, Brodmann's area 3b) of nonhuman primates, leading to the conclusion that sensory representations in S1 differ from those at the periphery in at least two important ways. First, while cutaneous nerve fibers can be divided into a small number of classes each responding to a different aspect of skin deformation (1–3), individual S1 neurons integrate sensory signals from multiple classes of nerve fibers (4–7). Indeed, while each class of nerve fibers exhibits stereotyped responses to certain stimulus classes, for example, skin indentations or sinusoidal vibrations, cortical responses to these same stimuli include features of the responses from multiple tactile classes or submodalities. Second, the responses of cortical neurons reflect computations on these inputs. For example, the spatial receptive fields (RFs) of S1 neurons comprise excitatory and inhibitory subfields, implying a spatial computation (8, 9). Similarly, S1 neurons act as temporal filters, as evidenced by the fact that their responses to vibrations reflect both integration and differentiation of their inputs in time (10). These computations give rise to increasingly explicit rate-based representations of object features, such as the orientation of an edge indented into the skin or the texture of a surface scanned across the skin (5, 8).

In contrast to the well-studied peripheral and cortical representations of touch, comparatively less is known about the contribution of the cuneate nucleus (CN) to the processing of tactile information. The textbook view is that the CN acts as a simple relay station despite the fact that the response properties of neurons in the CN or equivalent brain structures (e.g., nucleus principalis) exhibit responses that are not identical to those of nerve fibers (11–15), implying some processing. However, CN responses have not been investigated using stimuli whose representation in the nerve and cortex has been quantitatively characterized (12, 13, 16, 17). This precludes a quantitative analysis of how tactile signals are transformed in this structure.

To fill this gap, we recorded the responses evoked in individual CN neurons to a battery of tactile stimuli that have been extensively used to characterize the response properties of tactile nerve fibers and of neurons in S1, including skin indentations, vibrations, embossed dot patterns, and scanned edges. We then compared CN responses to their upstream (nerve fibers) and downstream counterparts [Brodmann's area 3b or S1, the first stage of processing in the cortex (18, 19)] to assess the degree to which tactile signals are processed in the CN. The picture that emerges is one in which the CN plays an integral part in the transformation of tactile information as it ascends the neuraxis.

Results

To investigate tactile representations in the CN, we measured the responses of individual CN neurons ($n = 33$) to step indentations, sinusoidal skin vibrations ($n = 68$), mechanical noise

Significance

Perception is the outcome of the sequential processing of sensory signals at multiple stages along the neuraxis. The conventional view is that tactile signals are processed predominantly in the cerebral cortex. We tested this view by investigating the response properties of neurons in the cuneate nucleus (CN), the first potential stage of processing along the primary touch neuraxis. We found that CN responses more closely resemble those of cortical neurons than they do those of nerve fibers: CN neurons have spatially complex receptive fields reflecting convergent input from multiple classes of nerve fibers and exhibit a selectivity for object features, absent in the nerve. We conclude that the CN plays a key, early role in the processing of tactile information.

Author contributions: A.K.S., C.M.G., L.E.M., and S.J.B. designed research; A.K.S., C.M.G., Q.H., J.M.R., and L.E.M. performed research; A.K.S., C.M.G., and Q.H. analyzed data; and A.K.S., C.M.G., Q.H., J.M.R., L.E.M., and S.J.B. wrote the paper.

The authors declare no competing interest.

This article is a PNAS Direct Submission.

[1]A.K.S. and C.M.G. contributed equally to this work.

[2]To whom correspondence may be addressed. Email: sliman@uchicago.edu.

This article contains supporting information online at http://www.pnas.org/lookup/suppl/doi:10.1073/pnas.2115772118/-/DCSupplemental.

Published December 1, 2021.

(n = 33), random dot patterns (n = 31), and scanned bars (n = 9). To compare CN responses to their peripheral counterparts, we analyzed previously collected afferent responses to skin indentations and simulated the spiking responses of tactile nerve fibers to the vibratory stimuli used in the CN recordings using a model that can reconstruct such responses with millisecond-level precision (20). To compare CN responses to their cortical counterparts, we analyzed previously collected cortical responses to analogous stimuli.

Adaptation Properties of CN Neurons Reveal Submodality Convergence. Nerve fibers can be readily divided into two groups based on their responses to skin indentations: Slowly adapting type 1 (SA1) fibers respond throughout the skin indentation, whereas rapidly adapting (RA) and Pacinian corpuscle–associated (PC) fibers respond only to the onset and offset of the indentation and are silent during the intermediate sustained epoch (6). Examination of the responses of downstream neurons to skin indentations can thus reveal the submodality composition of their inputs. Specifically, responses during the sustained component reflect SA1 input, as only this class is active during this stimulus epoch; a strong phasic response during the offset of the indentation is indicative of RA or PC input, as only these two classes of nerve fibers produce an off response. Co-occurrence of these two response properties reflects convergent input from at least two classes of nerve fibers. In the CN, we found that the responses of a majority of neurons comprise both sustained and off components, indicative of convergent input from multiple submodalities (Fig. 1*A*).

A previously developed "adaptation index" (AI, ref. 6) gauges the degree to which individual neurons receive convergent input from multiple cutaneous submodalities based on the relative strengths of the sustained and off responses. A value of 1 denotes RA-like responses (only an off response, no sustained response), a value of 0 denotes SA1-like responses (only a sustained response, no off response), and an intermediate value denotes convergent input (mixture of sustained and off responses). Adaptation indices computed on CN responses spanned the range from 0 to 1, with most falling between the two extremes, suggesting that convergence is the rule rather than the exception (Fig. 1*B*). Indeed, the AI distribution in the CN was equivalent to that in S1 (Kolmogorov–Smirnov test; D = 0.218 and $P = 0.19$) and significantly different from that at the periphery (KS test; D = 0.545 and $P < 0.001$). A greater number of neurons exhibited pure RA-like than SA1-like responses, as has been found in S1, commensurate with the relative densities of these two groups of nerve fibers (RA/PC versus SA1). To obtain a quantitative estimate of the proportion of multimodal neurons, we tested whether the firing rates during the sustained and offset periods were significantly different from the baseline period. Of the 33 neurons tested with skin indentations, 6% produced only sustained responses, 27% only offset responses, and 60% produced both sustained and offset responses (the remaining 7% only produced a transient onset response). Convergence of cutaneous submodalities is thus observed in a majority of neurons in the CN.

CN Responses to Vibrations Reveal Submodality Convergence. Next, we examined the responses of CN neurons to sinusoidal vibrations varying in amplitude and frequency, leveraging the fact that different afferent classes exhibit different frequency sensitivity: SA1 fibers peak in sensitivity at low frequencies, PC fibers at high frequencies, and RA fibers at intermediate frequencies (3, 21). We can then assess whether the frequency response characteristic of individual CN neurons resembles that of any single class of tactile nerve fiber or rather reflects convergent input from multiple fiber types. We found that some CN neurons respond exclusively to low frequencies,

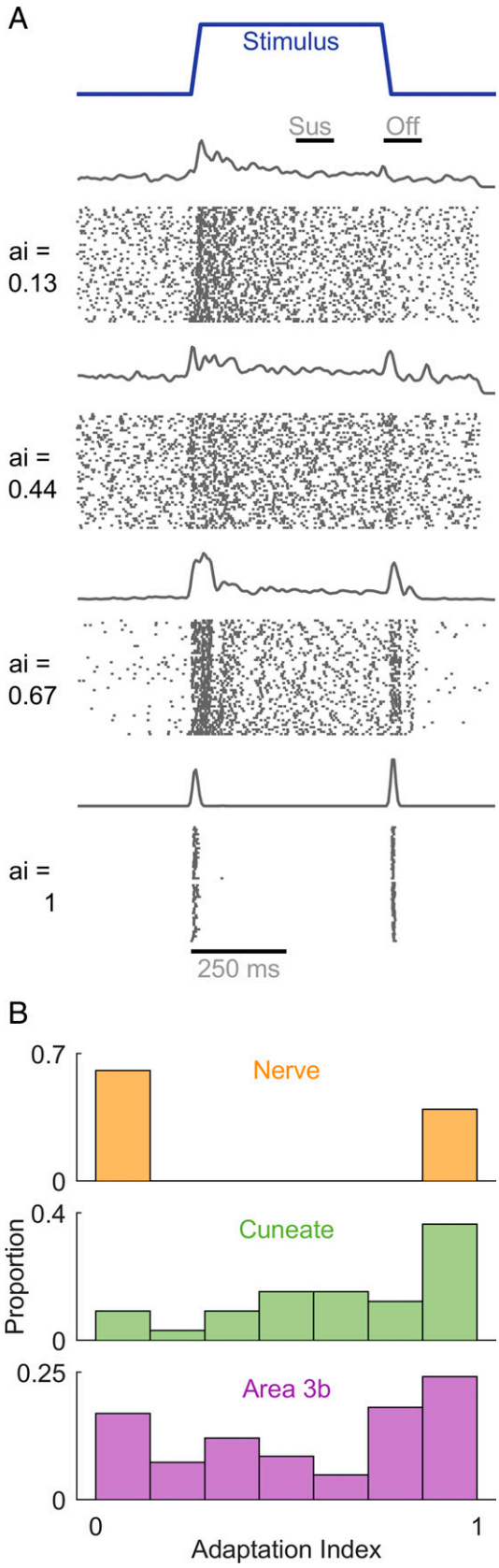

Fig. 1. CN responses to step indentations. (*A*) Responses of four CN neurons that span the range of convergence properties. (*B*) The AI for the nerve (*Top*), CN (*Middle*), and the primary somatosensory cortex (*Bottom*). AI segregates nerve fibers at the two extremes, whereas convergence is observed in both the CN and S1.

similar to SA1 fibers (Fig. 2*A*), and others to high frequencies, similar to PC fibers (Fig. 2*B*), but many respond to the entire range of frequencies tested (Fig. 2*C*), suggesting they receive convergent input from multiple tactile submodalities.

To quantitatively assess the contributions of different afferent classes to the responses of CN neurons, we regressed the firing rates of individual CN neurons onto the (simulated) population firing rates of nerve fibers from all three classes to a common set of vibrations (Fig. 3*A*). First, we verified that the responses of most CN neurons could be well accounted for using a linear combination of SA1, RA, and PC responses (mean $R^2 = 0.6$). Second, we assessed whether CN responses were better accounted for by multiple afferent classes than by one and found that, for most CN neurons, the cross-validated model fit increased significantly with the inclusion of all inputs (Fig. 3*A*; mean $R^2_{best} = 0.50$, mean $R^2_{all} = 0.60$, mean $\Delta R^2 = 0.1$, ranksum = 5,395, z = 3.2, and $P = 0.0013$). We repeated the regression analysis on measured responses of tactile nerve fibers to similar sinusoidal vibrations to verify our ability to distinguish unimodal from multimodal responses. We found that measured afferent responses to vibrations were equally well accounted for with a single modality as they were multiple modalities (Fig. 3*A*; mean $R^2_{best} = 0.83$, mean $R^2_{all} = 0.86$, mean $\Delta R^2 = 0.03$, ranksum = 1,019, z = 1.53, and $P = 0.126$). We found that 46% of CN neurons yielded ΔR^2 that were more than one SD away from the mean ΔR^2 obtained from nerve fibers, whereas only 10% of nerve fibers exceeded this threshold.

Third, we estimated the number of afferent inputs required to predict CN responses accurately. To this end, we simulated the responses of a population of nerve fibers and assessed our ability to predict the responses of individual CN neurons as we sequentially added simulated nerve fibers to the regression model (Fig. 3*B*). We found that model fits typically leveled off (reached criterion performance) with just two to five inputs if all three classes of nerve fibers were included in the analysis. If only the most predictive afferent class was included, more inputs were required to achieve equivalent fits and performance plateaued at a lower level, consistent with the analysis based on mean (simulated) population responses (Fig. 3*B*; dashed line). Including all three afferent classes as regressors significantly improved CN predictions (mean $\Delta R^2 = 0.06$ at criterion, ranksum = 5,518, z = 3.07, and $P = 0.002$). We validated the approach by verifying that including all three classes did not improve afferent predictions (mean $\Delta R^2 = 0.01$ at criterion, ranksum = 977, z = 0.90, and $P = 0.36$). Examination of the optimized regression coefficients revealed that 15% of CN neurons were unimodal, 59% were bimodal, and the remainder (26%) were trimodal (Fig. 3*C*). In conclusion, then, the responses of individual CN neurons to vibrations reflect input from multiple classes of nerve fibers, so the submodality convergence observed in the cortex is at least in part inherited from the CN.

CN Responses to Vibrations Reveal Temporal Computations. Neurons in the somatosensory cortex have been shown to exhibit a variety of response properties to vibrations (10). Some neurons sum their inputs over time, whereas others act as more complex temporal filters, comprising both excitatory and suppressive components. Examination of the rate-intensity functions for vibrations revealed suppressive components in the neuronal

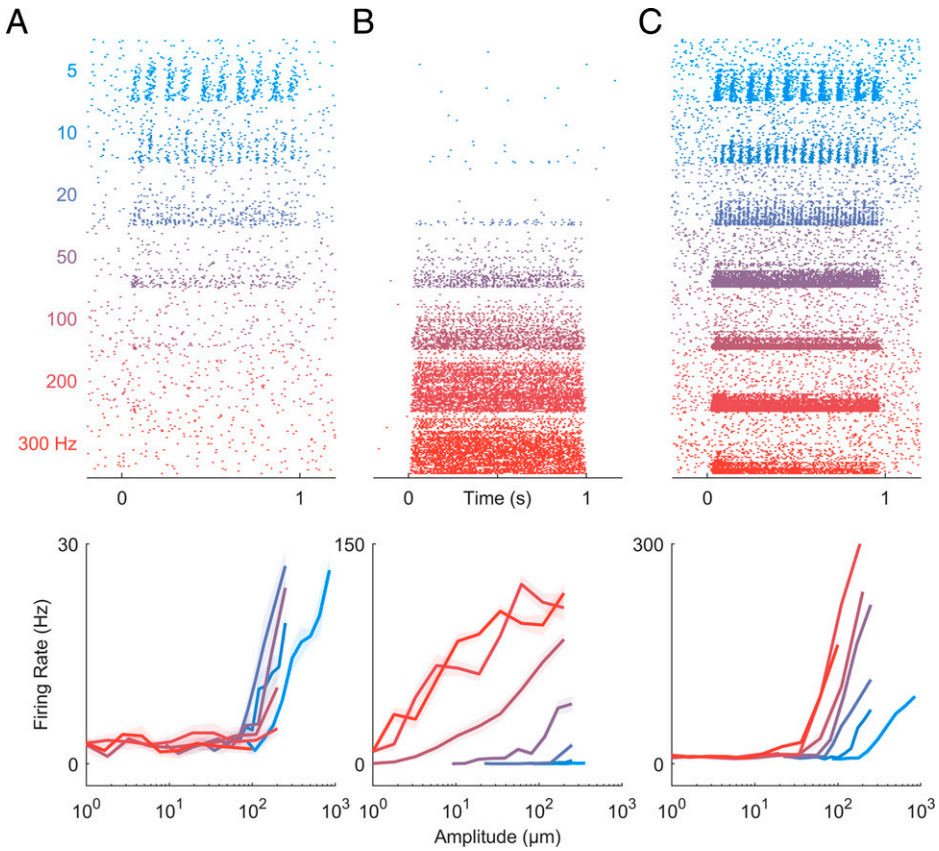

Fig. 2. CN responses to vibrations. (*A*–*C*) Responses of three CN neurons to skin vibrations varying in frequency (from 5 to 300 Hz) and amplitude (1 to 1,000 μm; ordered by frequency, then amplitude). Some CN neurons responded exclusively at low frequencies (*A*), others at high frequencies (*B*), but many CN neurons responded over a wider range of frequencies than any single population of nerve fibers (*C*). As is the case in the periphery and cortex, CN neurons often exhibited phase-locked responses to vibratory stimuli (*SI Appendix*, Fig. S1*C*).

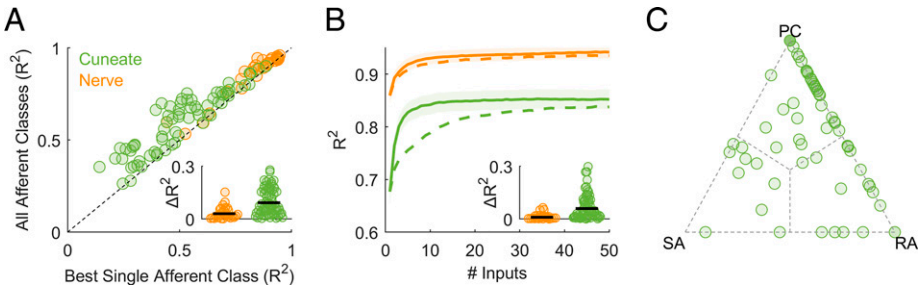

Fig. 3. CN responses to vibrations reflect convergent input from multiple afferents, typically of multiple classes. (*A*) Model fit with only one class of nerve fibers versus model fit with multiple classes for CN and afferents. The measured responses of nerve fibers can be predicted nearly perfectly from the simulated responses of a single afferent type, whereas CN neurons often require multiple. (*Inset*) Model improvement when allowing all classes is significantly greater for cuneate than individual afferents. For this analysis, the mean response to each stimulus is used as a regressor computed separately for each class of nerve fibers. (*B*) Performance of regression models as a function of the number of afferents included in the analysis. Input from two to five nerve fibers is sufficient to achieve asymptotic performance for CN predictions, but only if convergence across submodalities is allowed. When only the best single afferent class is used (dashed line), an order of magnitude more afferents are required to reach asymptotic performance. (*Inset*) At criterion, model performance is significantly improved when all afferent classes are included as regressors in models of CN responses. (*C*) Normalized regression weights for each afferent class; each point denotes a CN neuron.

response (*SI Appendix*, Fig. S1): Some CN neurons were always suppressed by vibration, whereas others were excited by some vibrations and suppressed by others. For these neurons, regression models yielded significantly poorer fits when weights were constrained to be positive (mean 22% decrease). These suppressive components may constitute building blocks of more complex temporal feature filtering.

To further characterize the process of temporal integration, we examined CN responses to mechanical noise. Specifically, we computed the mean response evoked in each afferent class immediately preceding each spike evoked in a given CN neuron (Fig. 4). The resulting spike-triggered averages (STAs) represent how a neuron integrates the signal from each population of nerve fibers. Some neurons simply summed their afferent input, whereas others exhibited more complex response properties, with STAs that comprised excitatory and suppressive components similar to those derived from S1 responses to analogous stimuli. As is the case in the cortex, PC input tended to be more suppressive than was RA or SA1 input (Fig. 4*C*). Temporal RFs that comprise excitatory and suppressive components confer to neurons a preference to fluctuations in the afferent input; heterogeneity in the filters across neurons and input classes (cf. ref. 10) gives rise to a high-dimensional rate-based representation of the input (5).

From CN responses to mechanical noise, we also estimated the mean latency in the CN to be around 10 ms (Fig. 4*D*), approximately half of that in S1 (~18 ms).

Spatial Structure of CN RFs. Neurons in the somatosensory cortex act not only as temporal filters (10) but also as spatial filters (5, 8, 9). The spatial RFs of S1 neurons comprise excitatory and inhibitory subfields, conferring to them a sensitivity to specific spatial features in their inputs. For example, an elongated excitatory subfield flanked by an inhibitory one will confer to a neuron a selectivity for orientation (8, 22).

With this in mind, we reconstructed the spatial RFs of CN neurons from their responses to random patterns of embossed dots scanned across the skin (cf. refs. 5 and 9). First, we found that the RFs of CN neurons tend to be larger than are those of SA1 or RA fibers (23) as expected, given the inferred

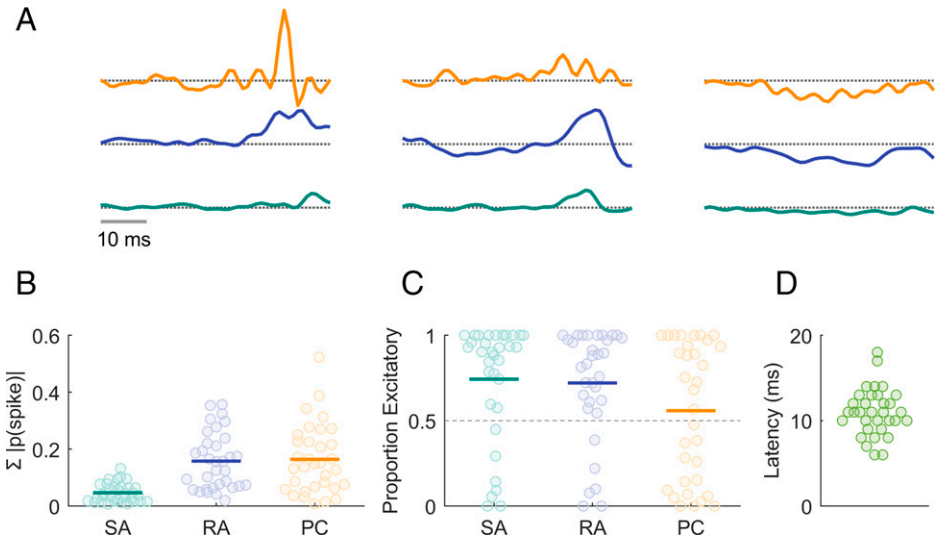

Fig. 4. Temporal integration properties of CN neurons. (*A*) STAs computed from the responses of three CN neurons for inputs from the three classes of nerve fibers. STAs comprise both excitatory and suppressive components, as do their counterparts derived from the responses of S1 neurons. (*B*) Summed absolute spike probability for each CN neuron with respect to afferent type. Given the frequency composition of the vibrations, the RA and PC drives were greater than the SA1 drive. (*C*) Proportion of the afferent input that is excitatory versus suppressive. The temporal RFs of many CN neurons included both excitatory and suppressive components. (*D*) The latency, estimated from responses to mechanical noise, was about half of that in S1.

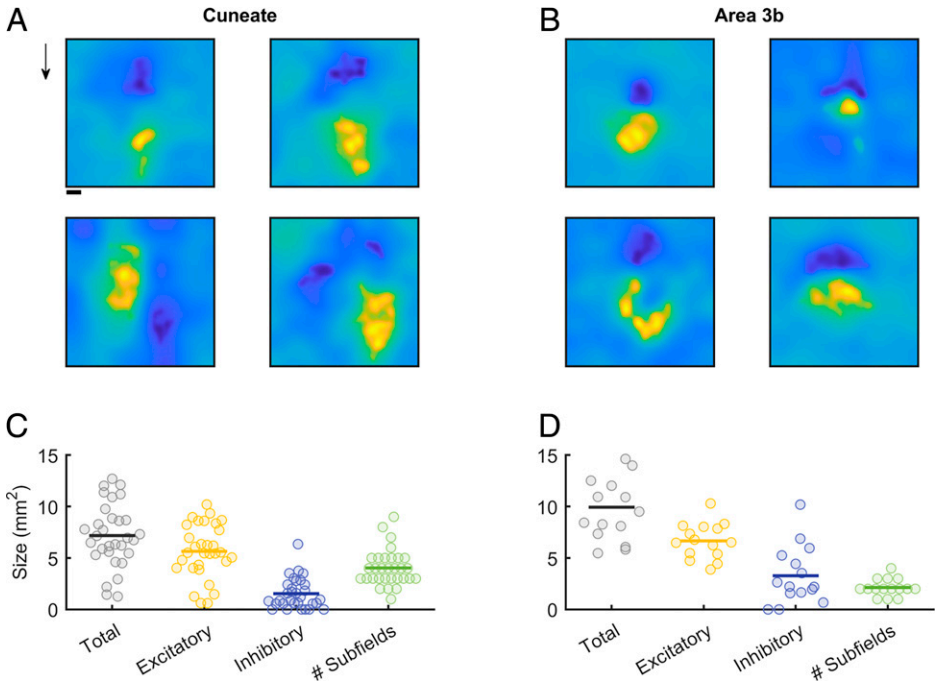

Fig. 5. Spatial RFs of CN neurons. (*A*) Reconstructed RFs for four CNs. RFs typically comprise both excitatory and inhibitory subfields in a variety of conformations. Cuneate RFs are thus similar to their S1 counterparts (*B*). Arrow indicates the direction in which the dot pattern was scanned. (Scale bar, 1 mm.) (*C*) Cuneate RFs are, on average, smaller than those in S1 (*D*), a difference that is primarily driven by smaller inhibitory subfields.

convergence of afferent input onto individual CN neurons (Fig. 5*A* and *C*). Second, CN neurons have marginally smaller RFs than do their cortical counterparts (Fig. 5*C* and *D*) as expected, given their relative positions along the neuraxis. The mean RF size is 7.2 mm^2 in the CN and 9.9 mm^2 in the cortex [*t* test: $t(44) = 2.8$; $P = 0.072$]. Third, CN neurons have complex RFs, often comprising excitatory and inhibitory subfields, like their cortical counterparts (Fig. 5*A* and *B*). As in the cortex, the excitatory subfields of CN neurons tend to be larger than their inhibitory counterparts. However, CN RFs tend to comprise a greater number of distinct subfields than do their S1 RFs [mean of 4 versus 2.1 mm^2; $t(44) = 4$; $P < 0.001$]. While the excitatory masses are similar in the CN and S1, the inhibitory masses are smaller in the CN than in S1 [excitatory: 5.6 versus 6.6 mm^2; $t(44) = 1.37$; $P = 0.178$; inhibitory: 1.5 versus 3.3 mm^2; $t(44) = 2.8$; $P < 0.008$]. Nonetheless, the spatial structure of the RFs observed in the CN is qualitatively similar to its counterpart in S1.

CN Neurons Exhibit Feature Selectivity. Next, we examined whether the spatial structure of RFs confer to the firing rate responses of CN neurons a selectivity for specific geometric features as it does in the cortex but not the periphery. To this end, we measured the responses of CN neurons to oriented edges scanned across their RFs. We found that the firing rates of a subset of CN neurons are modulated by orientation (Fig. 6*A* and *SI Appendix*, Fig. S2), responding more strongly to edges at some orientations than others. Some neurons are also modulated by direction of movement, responding strongly to a bar scanned in one direction but less so to the same bar scanned in the opposite direction (top right and bottom left neurons in Fig. 6*A*). We quantified the strength of the orientation tuning using a metric—the orientation selectivity index (OSI)—that takes on a value of 1 when a neuron responds only to a single orientation and 0 when it responds uniformly to all orientations. The degree of orientation selectivity in the CN is intermediate between that seen in the nerve—where none exists—and in the cortex (Fig. 6*B*). Therefore, the feature selectivity observed in the cortex is, to some extent, inherited from its inputs.

Discussion

The objective of the present study was to characterize the tactile representation in the CN and to assess the degree to which CN responses reflect computations on their inputs. To these ends, we probed CN responses using stimuli whose representation in the peripheral nerve has been extensively characterized, allowing us to disentangle derived response properties from those inherited from the inputs. Any difference between nerve and CN responses could then be attributed to computations within the CN [or possibly to an intervening synapse in the spinal cord (24–27)]. We found that CN neurons receive convergent input from multiple tactile submodalities, exhibit spatial and temporal filtering properties that had previously been attributed to cortical processing, and are tuned for behaviorally relevant object features. Comparison of CN responses to their upstream and downstream counterparts suggests that the tactile representation in the CN is more similar to its counterpart in the cortex than it is to that in the nerve.

Submodality Convergence. Tactile nerve fibers that innervate the glabrous skin of monkeys can be divided into three clearly delineated classes, each with distinct response properties (18). While each submodality might be more responsive to any one stimulus feature, information about most features is distributed over all three submodalities, and the resulting perceptual experience reflects this integration (7, 21, 28, 29). As might be expected, then, the responses of individual S1 neurons typically reflect convergent input from multiple classes of nerve fibers (6). Where this integration might first take place was unclear, however. Studies with cats suggested a lack of submodality convergence in the CN (11, 30–33), whereas studies in rodents conclude that the trigeminal nucleus—a structure analogous to the CN that receives inputs from the face—exhibits submodality convergence at the single-cell level (14, 34, 35).

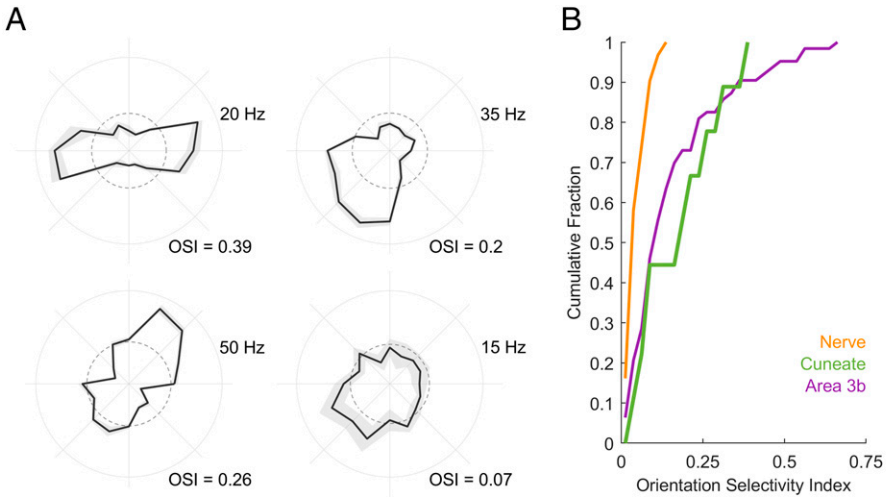

Fig. 6. Orientation tuning in CN neurons. (*A*) Response of four example CN neurons to oriented edges. The angular coordinate denotes orientation, the radial coordinate denotes firing rate, and the dashed circle denotes the firing rate averaged across conditions. (*B*) Cumulative distribution of the OSI derived from the responses of nerve fibers, CN neurons, and S1 neurons. CN responses are more strongly tuned for orientation than are nerve fibers but more weakly tuned than some S1 neurons.

Here, we show that the CN of primates features submodality convergence. Indeed, the majority of CN neurons produce both an SA1-like sustained response to the static component of a skin indentation and an RA/PC-like phasic response at the offset of the indentation. Furthermore, individual CN neurons tend to respond to a wider range of frequencies than do primary afferents of any one class. The submodality convergence observed in the somatosensory cortex is thus, at least in part, inherited from its inputs and begins at the earliest processing stage along the dorsal column-medial lemniscus pathway.

Neural Computations. Tactile nerve fibers have small RFs that consist of one or more excitatory hot spots (2, 36) and faithfully encode local skin deformations (20). In contrast, S1 neurons have larger RFs that comprise excitatory and inhibitory subfields (5, 8, 9), which confer to them a selectivity for spatial features in their inputs. Individual cortical neurons also act as temporal filters (10), which confers to them a selectivity for temporal features in their inputs. The idiosyncratic spatial and temporal filtering properties of individual S1 neurons give rise to a high-dimensional representation of the input in the somatosensory cortex, in which different features of grasped objects are explicitly encoded (5, 8, 9, 37, 38)

Here, we show that the spatial and temporal computations observed in the cortex are also observed in the CN. First, the spatial RFs of CN neurons comprise excitatory and inhibitory subfields and, while somewhat smaller (as expected, since the CN is upstream from the cortex), resemble their cortical counterparts. Second, individual CN neurons process time-varying inputs in a variety of different ways—ranging from integration to differentiation—that are analogous to their cortical counterparts. The CN thus contributes to the processing of sensory information, and CN neurons exhibit response properties that are qualitatively similar to their counterparts in S1. We speculate that sensory signals undergo further transformations in the thalamus, the next stage of processing along the dorsal column-medial lemniscus pathway. More broadly, we hypothesize that the CN and the thalamus are integral components to the genesis of sensory representations that are suited to guide behavior.

Feature Selectivity. The spatiotemporal response properties of S1 neurons confer to them a preference for certain stimulus features. For example, individual S1 neurons exhibit a selectivity for the direction in which objects move across the skin (38, 39) or idiosyncratic preferences for different surface textures (5). Another well-documented feature selectivity in S1 is for oriented edges: A large proportion of S1 neurons respond preferentially to edges at a specific orientation (8). This orientation selectivity is attributed to the neuron's RF structure, which comprises excitatory and inhibitory subfields, analogous to neurons in the primary visual cortex (22). We show that CN neurons also exhibit orientation selectivity, suggesting that some of the feature selectivity observed in S1 is inherited from its inputs.

Feature extraction results in a sparsening of the stimulus representation, which can result in an overall loss of information (40), unless it is accompanied by an expansion of the size of the neuronal population (41). Not surprisingly, the CN is estimated to comprise three to five times more neurons than there are nerve fibers that innervate the corresponding dermatomes, with a preferential expansion of the representation of the hand (42–45), also reflected in S1 (43) and consistent with observations in other animals (17, 46, 47). The expanded neuronal representation in the CN is consistent with its role in feature extraction.

Conclusions. The naive textbook story is that the CN is a simple relay station that does not effect any computations on its inputs but rather transmits them unprocessed. The putative role of the CN, if any, has been to provide an opportunity to modulate the gain of the afferent input depending on its behavioral relevance via top-down signals (16, 48). In addition, plastic changes in the CN following amputation account for the resulting changes in activation patterns in somatosensory cortex (26, 49–52). We show that, in addition to this gain modulation and susceptibility to plasticity, the responses of CN neurons reflect a significant transformation of their afferent inputs, conferring to them properties that were heretofore attributed solely to the cortex. The CN is thus an active contributor to the process by which ambiguous signals from the periphery are converted into sensory representations that support robust and meaningful percepts and guide behavior.

Methods

Neurophysiology.

Animals and surgical preparation. Neuronal responses were obtained from seven rhesus macaques (five males and two females, 4 to 14 y of age, 4 to 12 kg). Monkeys were anesthetized and placed in a stereotaxic frame with their neck flexed at 90 degrees to provide access to the dorsal brain stem. The foramen magnum was exposed, and the inferior aspect of the occipital bone was removed. The dura above the obex was resected to reveal the brain stem. All

surgical procedures were approved and monitored by the Institutional Animal Care and Use Committee and were consistent with federal guidelines. The neurophysiological methods for the cortical and nerve fiber responses have been previously described (6, 8, 53).

Neurophysiological recordings. Neuronal activity was monitored using 16-channel linear probes (V-Probe, Plexon) and amplified and stored using a Cerebus system (Blackrock Microsystems). Probes were positioned with a stereotaxic system, using the obex as a landmark to locate the CN. Units with RFs on the glabrous surface of the hand were isolated. Responses from 143 neurons were obtained across experimental conditions. Hand mapping revealed that the majority of isolated units had small RFs, confined to a single digit pad or palmar whorl, with the exception of neurons that exhibited PC-like responses.

Anesthesia. All animals were induced with a combination of ketamine, dexmedetomidine, and buprenorphine. Isoflurane (1 to 2%) was then delivered continuously via inhalation and decreased during the neurophysiological recordings. While anesthesia can have a profound impact on neural responses (54–58), several observations suggest that the CN recordings were only minimally impacted. First, the impact of anesthesia tends to be more pronounced in the cortex (59). Given that the CN is the first recipient of afferent input itself minimally affected by anesthesia (60), the impact of anesthesia on CN responses, at least those driven by peripheral input, is likely minimal. Second, certain anesthetics have been shown to affect the temporal response properties of neurons in the cortex (55). That we observe precise and repeatable phase locking of CN responses to vibrations (*SI Appendix*, Fig. S1*C*) suggests that the anesthesia did not affect the temporal precision of the responses. Third, the CN has been shown to receive projections from the cortex (16, 48), and this top-down drive is almost certainly abolished or at least strongly altered under anesthesia. Note, however, that the cortical modulation of cutaneous responses in the CN seems to be primarily suppressive (16) under conditions for which this input may be disruptive (61). The similarity between the responses of CN neurons under anesthesia and those of S1 neurons monitored in awake animals implies that CN responsivity is relatively unaffected by anesthesia. Finally, in a previous series of experiments described in ref. 62, we recorded responses of three CN neurons to sinusoidal vibrations and found that vibratory thresholds were qualitatively similar (*SI Appendix*, Fig. S3).

Tactile Stimulation. We presented five classes of stimuli–skin indentations, sinusoidal vibrations, bandpass mechanical noise, scanned random dot patterns, and scanned edges—each with precisely controlled speed, force, frequency, and/or amplitude. In some cases, multiple stimulus classes were delivered while recording from a given neuron. Indentations, sinusoids, and noise stimuli were delivered with a probe (diameter = 1 mm) driven by a custom shaker motor (63) and preindented 0.5 mm into the skin. Scanned random dots and edges were presented using a miniaturized version of the drum stimulator (5, 29). Edges were presented using a custom stimulator that can scan stimuli across the skin in different directions and whose third degree of freedom allows for indentation into and retraction from the skin (see ref. 64). Responses to skin indentation and sinusoids were collected from four monkeys (number of neurons = 33 and 68, respectively), responses to bandpass noise and random dot patterns from two monkeys (n = 33 and 31), and responses to edges from one monkey (n = 9).

Skin indentations. The amplitude of the ramp and hold indentation was 1 mm, and their overall duration was 0.5 s, with on and off and ramps lasting 25 ms and separated by a 0.5-s interval. Indentations were presented 100 times.

Sinusoids. Sinusoidal vibrations were delivered at seven frequencies (5 to 300 Hz) and 10 amplitudes, which spanned the achievable range at each frequency, given the limitations of the stimulator. Each frequency–amplitude combination, lasting 1 s, was presented five times in pseudorandom order, separated by a 1-s interstimulus interval, for a total of 350 trials.

Bandpass mechanical noise. White Gaussian noise was filtered with different high and low pass frequencies (low: 5 to 50 Hz; high: 10 to 200 Hz) to yield 10 unique stimuli (as previously described in ref. 21), each lasting 1 s and separated by a 0.3-s interval.

Scanned random dot patterns. Random dot patterns were printed (Form 2, Formlabs) on a drum (2.5-in diameter) using previously used geometries and densities (cf. refs. 5 and 9). Patterns were repeatedly scanned across the skin at 80 mm/s. For the first scan, the edge of the pattern was aligned with the estimated center of the RF and indented into the skin by 0.5 mm. For each of 100 subsequent scans, the drum was progressively translated by 0.4 mm along the axis perpendicular to the axis of rotation.

Scanned edges. An edge (1-mm high, 1-mm wide, 0.25-mm chamfer) was printed on a miniature drum (40-mm diameter), whose rotation was driven by a rotational motor. The orientation of the drum on the skin was controlled by a second rotational motor. A third motor controlled the vertical excursion of the drum and allowed for it to be lifted in between changes in orientation. The edge was scanned five times at 80 mm/s at each of 16 orientations (0 to 337.5 degrees with 22.5-degree spacing).

Data Analysis.

Adaptation index. The adaptation index (6) indicates the relative firing rate of the sustained and offset periods. SA1 afferents respond to the onset and sustained period, while RA and PC afferents respond to the onset and offset transient periods. Thus, the submodality composition of the inputs of a downstream neuron can be measured by taking the ratio of the offset and sustained period. The baseline firing rate was subtracted from both the computed sustained (fr_{sus}) and offset (fr_{off}) firing rates (measured between 0.275 and 0.375 and 0.505 and 0.605 s, respectively). The adaptation index was then computed as follows:

$$ai = \mid tan^{-1}\left(\frac{fr_{off}}{fr_{sus}}\right) * \frac{2}{\pi} \mid .$$

Afferent convergence. Given that each class of nerve fibers exhibits a unique frequency response characteristic, we sought to determine if the cuneate responses could be explained by linear combinations of inputs from the three afferent classes. To this end, we simulated the responses of each afferent type to the sinusoidal stimuli used in this study. For this, we used TouchSim, a model that yields millisecond precision reconstructions of the responses of every tactile nerve fiber that innervates the glabrous skin of the hand to arbitrary stimuli delivered to the skin (20). The firing rates evoked by each stimulus were then averaged across afferents of the same type. For each cuneate neuron, we used linear regression in the following form:

$$fr_{cn} = \varphi_0 + \varphi_1 fr_{SA1} + \varphi_2 fr_{ra} + \varphi_3 fr_{pc}.$$

We compared the performance of the full model to that of models that only included one class of nerve fibers. We assessed model performance using five-fold cross-validation to ensure that models with more parameters did not outperform simpler models due to overfitting. We then compared the best-performing single-afferent model to that of the full model for each neuron.

To estimate the number of afferents that contribute to the CN response, we performed a regression analysis using the firing rates of individual nerve fibers as regressors. We then used a stepwise linear regression process to determine the optimal combination of inputs. Briefly, on the first iteration, we selected the nerve fiber that had the highest correlation with the CN response. During each subsequent step, we measured the increase in correlation when adding every other afferent in the population, either across classes or within class. We then incorporated the fiber that most improved the regression performance. We proceeded until the addition of an additional regressor failed to improve the model fit more than 5%. To determine the relative contributions of each afferent type to the CN response, we summed the absolute regression coefficient within afferent type and normalized by the summed absolute regression values across afferent types.

Spike-triggered average—transfer function. Responses to mechanical noise can be used to estimate the transfer function of a neuron (10, 65). Accordingly, we simulated the responses of all the nerve fibers that innervate the glabrous skin of the hand to the bandpass mechanical noise used in the neurophysiological experiments and averaged their responses across fibers of each class. We then performed an STA (65) of the response of each afferent conditioned on each spike in the CN. That is, the response of each afferent population over the 100 ms preceding each CN spike was averaged across CN spikes. The resulting filter was smoothed using a Gaussian filter (SD = 5 ms), and the baseline firing rate was subtracted. We then standardized the resultant filter for each cuneate–afferent pair with respect to the period between 100 and 50 ms before the cuneate spike, which we expect to reflect noise. We then thresholded ($z > 2$) the z-scored probabilities and computed the magnitude and width of the filters.

Harmonic ratio. To determine the extent to which CN responses to sinusoids were phase locked, we computed the harmonic ratio of the response to each stimulus. Excluding responses with fewer than five spikes, we performed a Fast Fourier transform of the peristimulus spike histogram (binned at 1/5f), averaged the mean amplitude at the fundamental frequency (A_f) and its first harmonic (A_{h1}), and divided the resulting value by the median amplitude across all frequencies ($\tilde{A}$):

$$hr = \frac{(A_f + A_{h1})/2}{\tilde{A}},$$

where

$$A = \mid real[FFT(x)] + imag[FFT(x)] \mid * 1/fs.$$

We repeated this analysis for Poisson spike trains to obtain a distribution of harmonic ratios for responses that lack periodicity.

NEUROSCIENCE

Spatial RFs. We used standard techniques to estimate the spatial RF of each cuneate neuron (cf. refs. 5 and 9). In brief, we averaged the 16 mm × 16 mm swath of the random dot pattern that impinged on the skin at the time of each cuneate spike. To remove the curvature of the drum reflected in the resulting STA, we subtracted a second-order polynomial plane from it. The resultant STA was then standardized and thresholded to isolate excitatory and inhibitory lobes.

To identify the number of subfields for cortical and cuneate RFs, we fitted two-dimensional Gaussians to each RF. Each Gaussian subfield had the following form:

$$G(x, y) = a \cdot e^{(-\frac{1}{2}(L\Sigma^{-1}L^T))},$$

where $L = \left[x - \mu_x,\ y - \mu_y\right]$, $\Sigma = \mathrm{CovMat}(\sigma_x, \sigma_y, \theta)$, a is the amplitude ($a > 0$ denotes an excitatory patch, $a < 0$ an inhibitory one), (x, y) denote the medial–lateral and proximal–distal locations on the skin surface, respectively, (μ_x, μ_y) represent the center of the Gaussian, (σ_x, σ_y) its SDs along the two axes, and θ its orientation.

Therefore, every RF is described by a total of $N \times 6$ parameters (six parameters for each Gaussian component: $a, \mu_x, \mu_y, \sigma_x, \sigma_y$, and θ; and N Gaussian components). Nonlinear least-squares optimization was used to find the best parameters. N represents the minimum number of Gaussian subfields needed to achieve $R^2 > 0.9$ of 90% of the maximum achievable R^2.

Orientation tuning. Spiking responses evoked at each orientation were aligned to a reference stimulus trace consisting of six Gaussians spaced according to the stimulus speed. The spike rate evoked by the stimulus, centered around the peak response, was averaged over a window of 314 ms, corresponding to 6.2 mm of travel (5% of a complete rotation of the drum), though the window size did not affect the results over a wide range (*SI Appendix*, Fig. S2). The tuning of each neuron was gauged using an orientation selectivity index (OSI), given by

$$OSI = \frac{\sqrt{\sum(R_\varphi * \sin(2\varphi))^2 + (R_\varphi * \cos(2\varphi))^2}}{\sum R_\varphi},$$

where φ is the orientation of the stimulus and R_φ is the firing rate at that orientation. Reliability of the OSI was tested using a permutation test, for which neural responses were shuffled 10,000 times and the OSI recomputed.

Data Availability. All data and code for analyses and generation or figures can be found at Figshare (https://doi.org/10.6084/m9.figshare.15054294.v1) (66) .

ACKNOWLEDGMENTS. We thank Amit Ayer for help with the surgical procedures. This work was supported by National Institute of Neurological Disorders and Stroke Grants NS122333 (S.J.B.), NS095162 (J.M.R., L.E.M., S.J.B.), and NS096952 (A.K.S.).

1. J. M. Goodman, S. J. Bensmaia, "The neural mechanisms of touch and proprioception at the somatosensory periphery" in *The Senses,* B. Fritzsch, Ed. (Elsevier, 2020), pp. 2–27.
2. R. S. Johansson, Tactile sensibility in the human hand: Receptive field characteristics of mechanoreceptive units in the glabrous skin area. *J. Physiol.* **281**, 101–125 (1978).
3. W. H. Talbot, I. Darian-Smith, H. H. Kornhuber, V. B. Mountcastle, The sense of flutter-vibration: Comparison of the human capacity with response patterns of mechanoreceptive afferents from the monkey hand. *J. Neurophysiol.* **31**, 301–334 (1968).
4. J. Hyvärinen, A. Poranen, Receptive field integration and submodality convergence in the hand area of the post-central gyrus of the alert monkey. *J. Physiol.* **283**, 539–556 (1978).
5. J. D. Lieber, S. J. Bensmaia, High-dimensional representation of texture in somatosensory cortex of primates. *Proc. Natl. Acad. Sci. U.S.A.* **116**, 3268–3277 (2019).
6. Y.-C. Pei, P. V. Denchev, S. S. Hsiao, J. C. Craig, S. J. Bensmaia, Convergence of submodality-specific input onto neurons in primary somatosensory cortex. *J. Neurophysiol.* **102**, 1843–1853 (2009).
7. H. P. Saal, S. J. Bensmaia, Touch is a team effort: Interplay of submodalities in cutaneous sensibility. *Trends Neurosci.* **37**, 689–697 (2014).
8. S. J. Bensmaia, P. V. Denchev, J. F. Dammann III, J. C. Craig, S. S. Hsiao, The representation of stimulus orientation in the early stages of somatosensory processing. *J. Neurosci.* **28**, 776–786 (2008).
9. J. J. DiCarlo, K. O. Johnson, S. S. Hsiao, Structure of receptive fields in area 3b of primary somatosensory cortex in the alert monkey. *J. Neurosci.* **18**, 2626–2645 (1998).
10. H. P. Saal, M. A. Harvey, S. J. Bensmaia, Rate and timing of cortical responses driven by separate sensory channels. *eLife* **4**, e10450 (2015).
11. E. Bystrzycka, B. S. NAil, M. Rowe, Inhibition of cuneate neurones: Its afferent source and influence on dynamically sensitive "tactile" neurones. *J. Physiol.* **268**, 251–270 (1977).
12. C. Ebert, K. Bagdasarian, S. Haidarliu, E. Ahissar, A. Wallach, Interactions of whisking and touch signals in the rat brainstem. *J. Neurosci.* **41**, 4826–4839 (2021).
13. H. Jörntell *et al.*, Segregation of tactile input features in neurons of the cuneate nucleus. *Neuron* **83**, 1444–1452 (2014).
14. A. S. Kaloti *et al.*, Representation of stimulus speed and direction in vibrissal-sensitive regions of the trigeminal nuclei: A comparison of single unit and population responses. *PLoS One* **11**, e0158399 (2016).
15. C. L. Witham, S. N. Baker, Modulation and transmission of peripheral inputs in monkey cuneate and external cuneate nuclei. *J. Neurophysiol.* **106**, 2764–2775 (2011).
16. J. M. Conner *et al.*, Modulation of tactile feedback for the execution of dexterous movement. bioRxiv [Preprint] (2021). https://doi.org/10.1101/2021.03.04.433649.
17. B. P. Lehnert *et al.*, Mechanoreceptor synapses in the brainstem shape the central representation of touch. bioRxiv [Preprint] (2021). https://doi.org/10.1101/2021.02.02.429463 (Accessed 13 August 2021).
18. B. P. Delhaye, K. H. Long, S. J. Bensmaia, Neural basis of touch and proprioception in primate cortex. *Compr. Physiol.* **8**, 1575–1602 (2018).
19. J. H. Kaas, What, if anything, is SI? Organization of first somatosensory area of cortex. *Physiol. Rev.* **63**, 206–231 (1983).
20. H. P. Saal, B. P. Delhaye, B. C. Rayhaun, S. J. Bensmaia, Simulating tactile signals from the whole hand with millisecond precision. *Proc. Natl. Acad. Sci. U.S.A.* **114**, E5693–E5702 (2017).
21. M. A. Muniak, S. Ray, S. S. Hsiao, J. F. Dammann, S. J. Bensmaia, The neural coding of stimulus intensity: Linking the population response of mechanoreceptive afferents with psychophysical behavior. *J. Neurosci.* **27**, 11687–11699 (2007).
22. D. H. Hubel, T. N. Wiesel, Receptive fields, binocular interaction and functional architecture in the cat's visual cortex. *J. Physiol.* **160**, 106–154 (1962).
23. K. O. Johnson, G. D. Lamb, Neural mechanisms of spatial tactile discrimination: Neural patterns evoked by braille-like dot patterns in the monkey. *J. Physiol.* **310**, 117–144 (1981).
24. V. E. Abraira, D. D. Ginty, The sensory neurons of touch. *Neuron* **79**, 618–639 (2013).
25. G. J. Giesler Jr., R. L. Nahin, A. M. Madsen, Postsynaptic dorsal column pathway of the rat. I. Anatomical studies. *J. Neurophysiol.* **51**, 260–275 (1984).
26. C.-C. Liao, G. E. DiCarlo, O. A. Gharbawie, H.-X. Qi, J. H. Kaas, Spinal cord neuron inputs to the cuneate nucleus that partially survive dorsal column lesions: A pathway that could contribute to recovery after spinal cord injury. *J. Comp. Neurol.* **523**, 2138–2160 (2015).
27. A. J. Loutit, R. M. Vickery, J. R. Potas, Functional organization and connectivity of the dorsal column nuclei complex reveals a sensorimotor integration and distribution hub. *J. Comp. Neurol.* **529**, 187–220 (2021).
28. J. D. Lieber, X. Xia, A. I. Weber, S. J. Bensmaia, The neural code for tactile roughness in the somatosensory nerves. *J. Neurophysiol.* **118**, 3107–3117 (2017).
29. A. I. Weber *et al.*, Spatial and temporal codes mediate the tactile perception of natural textures. *Proc. Natl. Acad. Sci. U.S.A.* **110**, 17107–17112 (2013).
30. P. R. Douglas, D. G. Ferrington, M. Rowe, Coding of information about tactile stimuli by neurones of the cuneate nucleus. *J. Physiol.* **285**, 493–513 (1978).
31. D. G. Ferrington, S. Horniblow, M. J. Rowe, Temporal patterning in the responses of gracile and cuneate neurones in the cat to cutaneous vibration. *J. Physiol.* **386**, 277–291 (1987).
32. B. D. Gynther, R. M. Vickery, M. J. Rowe, Transmission characteristics for the 1:1 linkage between slowly adapting type II fibers and their cuneate target neurons in cat. *Exp. Brain Res.* **105**, 67–75 (1995).
33. R. M. Vickery, B. D. Gynther, M. J. Rowe, Synaptic transmission between single slowly adapting type I fibres and their cuneate target neurones in cat. *J. Physiol.* **474**, 379–392 (1994).
34. B. S. Minnery, R. M. Bruno, D. J. Simons, Response transformation and receptive-field synthesis in the lemniscal trigeminothalamic circuit. *J. Neurophysiol.* **90**, 1556–1570 (2003).
35. K. Sakurai *et al.*, The organization of submodality-specific touch afferent inputs in the vibrissa column. *Cell Rep.* **5**, 87–98 (2013).
36. F. Vega-Bermudez, K. O. Johnson, SA1 and RA receptive fields, response variability, and population responses mapped with a probe array. *J. Neurophysiol.* **81**, 2701–2710 (1999).
37. J. D. Lieber, S. J. Bensmaia, Emergence of an invariant representation of texture in primate somatosensory cortex. *Cereb. Cortex* **30**, 3228–3239 (2020).
38. Y.-C. Pei, S. S. Hsiao, J. C. Craig, S. J. Bensmaia, Shape invariant coding of motion direction in somatosensory cortex. *PLoS Biol.* **8**, e1000305 (2010).
39. E. P. Gardner, R. M. Costanzo, Neuronal mechanisms underlying direction sensitivity of somatosensory cortical neurons in awake monkeys. *J. Neurophysiol.* **43**, 1342–1354 (1980).
40. B. Babadi, H. Sompolinsky, Sparseness and expansion in sensory representations. *Neuron* **83**, 1213–1226 (2014).
41. P. M. Daniel, D. Whitteridge, The representation of the visual field on the cerebral cortex in monkeys. *J. Physiol.* **159**, 203–221 (1961).
42. M. A. Biedenbach, Cell density and regional distribution of cell types in the cuneate nucleus of the rhesus monkey. *Brain Res.* **45**, 1–14 (1972).
43. G. Corniani, H. P. Saal, Tactile innervation densities across the whole body. *J. Neurophysiol.* **124**, 1229–1240 (2020).

44. C. Darian-Smith, M. Ciferri, Cuneate nucleus reorganization following cervical dorsal rhizotomy in the macaque monkey: Its role in the recovery of manual dexterity. *J. Comp. Neurol.* **498**, 552–565 (2006).
45. J. Xu, J. T. Wall, Functional organization of tactile inputs from the hand in the cuneate nucleus and its relationship to organization in the somatosensory cortex. *J. Comp. Neurol.* **411**, 369–389 (1999).
46. K. C. Catania, D. B. Leitch, D. Gauthier, A star in the brainstem reveals the first step of cortical magnification. *PLoS One* **6**, e22406 (2011).
47. H. Wässle, U. Grünert, J. Röhrenbeck, B. B. Boycott, Retinal ganglion cell density and cortical magnification factor in the primate. *Vision Res.* **30**, 1897–1911 (1990).
48. K. J. Berkley, R. J. Budell, A. Blomqvist, M. Bull, Output systems of the dorsal column nuclei in the cat. *Brain Res.* **396**, 199–225 (1986).
49. P. Halder, N. Kambi, P. Chand, N. Jain, Altered expression of reorganized inputs as they ascend from the cuneate nucleus to cortical area 3b in monkeys with long-term spinal cord injuries. *Cereb. Cortex* **28**, 3922–3938 (2018).
50. N. Kambi *et al.*, Large-scale reorganization of the somatosensory cortex following spinal cord injuries is due to brainstem plasticity. *Nat. Commun.* **5**, 3602 (2014).
51. C.-C. Liao, J. L. Reed, H.-X. Qi, E. K. Sawyer, J. H. Kaas, Second-order spinal cord pathway contributes to cortical responses after long recoveries from dorsal column injury in squirrel monkeys. *Proc. Natl. Acad. Sci. U.S.A.* **115**, 4258–4263 (2018).
52. H.-X. Qi, O. A. Gharbawie, K. W. Wynne, J. H. Kaas, Impairment and recovery of hand use after unilateral section of the dorsal columns of the spinal cord in squirrel monkeys. *Behav. Brain Res.* **252**, 363–376 (2013).
53. M. A. Harvey, H. P. Saal, J. F. Dammann III, S. J. Bensmaia, Multiplexing stimulus information through rate and temporal codes in primate somatosensory cortex. *PLoS Biol.* **11**, e1001558 (2013).
54. B. Calancie, K. J. Klose, S. Baier, B. A. Green, Isoflurane-induced attenuation of motor evoked potentials caused by electrical motor cortex stimulation during surgery. *J. Neurosurg.* **74**, 897–904 (1991).
55. S. W. Cheung *et al.*, Auditory cortical neuron response differences under isoflurane versus pentobarbital anesthesia. *Hear. Res.* **156**, 115–127 (2001).
56. T. Noda, H. Takahashi, Anesthetic effects of isoflurane on the tonotopic map and neuronal population activity in the rat auditory cortex. *Eur. J. Neurosci.* **42**, 2298–2311 (2015).
57. K. K. Sellers, D. V. Bennett, A. Hutt, J. H. Williams, F. Fröhlich, Awake vs. anesthetized: Layer-specific sensory processing in visual cortex and functional connectivity between cortical areas. *J. Neurophysiol.* **113**, 3798–3815 (2015).
58. V. Shumkova, V. Sitdikova, I. Rechapov, A. Leukhin, M. Minlebaev, Effects of urethane and isoflurane on the sensory evoked response and local blood flow in the early postnatal rat somatosensory cortex. *Sci. Rep.* **11**, 9567 (2021).
59. M. T. Alkire, A. G. Hudetz, G. Tononi, Consciousness and anesthesia. *Science* **322**, 876–880 (2008).
60. J.-W. Cheng, A. I. Weber, S. J. Bensmaia, Comparing the effects of isoflurane and pentobarbital on the responses of cutaneous mechanoreceptive afferents. *BMC Anesthesiol.* **13**, 10 (2013).
61. Q. He *et al.*, Movement gating of cutaneous signals in the cuneate nucleus. bioRxiv [Preprint] (2019). https://doi.org/10.1101/2021.11.15.468735 (Accessed 19 November 2021).
62. A. K. Suresh *et al.*, Methodological considerations for a chronic neural interface with the cuneate nucleus of macaques. *J. Neurophysiol.* **118**, 3271–3281 (2017).
63. G. Westling, R. Johansson, Å. B. Vallbo, "A method for mechanical stimulation of skin receptors" in *Sensory Functions of the Skin in Primates*, Y. Zotterman, Ed. (Pergamon, 1976), pp. 151–158.
64. Y.-C. Pei *et al.*, A multi-digit tactile motion stimulator. *J. Neurosci. Methods* **226**, 80–87 (2014).
65. O. Schwartz, J. W. Pillow, N. C. Rust, E. P. Simoncelli, Spike-triggered neural characterization. *J. Vis.* **6**, 484–507 (2006).
66. C. Greenspon, S. Bensmaia, Dataset: Sensory computations in the cuneate nucleus of macaques. Figshare. https://doi.org/10.6084/m9.figshare.15054294.v1. Deposited 15 November 2021.